भारतीय प्रौद्योगिकी संस्थान गुवाहाटी

INDIAN INSTITUTE OF TECHNOLOGY GUWAHATI

Preparation Of Schrodinger Cat States : A Comprehensive Study

A M. Sc Project Report Submitted
in Partial Fulfillment of the Requirements
for the Degree of

Master of Scince

Submitted by

Akash Vaishnav

(212121005)

UNDER THE GUIDANCE OF

Prof. Amarendra Kumar Sarma

to the

DEPARTMENT OF PHYSICS

INDIAN INSTITUTE OF TECHNOLOGY GUWAHATI
GUWAHATI - 781039, ASSAM

CERTIFICATE

*This is to certify that the work contained in this thesis entitled "**"Preparation Of Schrodinger Cat States : A Comprehensive Study**" is a bonafide work of **Akash Vaishnav (Roll No. 212121005)**, carried out in the Department of Physics Indian Institute of Technology Guwahati under my supervision and that it has not been submitted elsewhere for a degree.*

Supervisor: **Professor Amarendra Kumar Sarma**

April,2023
Guwahati.

Department of Physics
Indian Institute of Technology Guwahati, Assam.

Acknowledgements

I would like to take this opportunity to express my sincere gratitude to Professor Amarendra Kumar Sarma for their guidance and support throughout my project. Their expertise and feedback were instrumental in the successful completion of this work.

I would also like to extend my heartfelt thanks to my teaching assistant, Urmimala Dewan, for providing me with valuable direction and assistance during this project. Her insights, suggestions, and encouragement were greatly appreciated.

Thank you all for your invaluable contributions and support.

Abstract

This study investigates the preparation of photonic Schrödinger cat states using three protocols in solid-state quantum dot-cavity (QDC) and atom-cavity systems, with potential applications in quantum information processing and communication. The first two protocols (DOD and CAD) for QDC Schrödinger cat state preparation rely heavily on the timing and mutual phases of laser pulses and suffer from radiative decay, cavity losses, and environmental coupling. The CAD protocol successfully prepares Schrödinger cat states in QDCs, while the DOD protocol is unsuitable due to detrimental effects. The third protocol for atom-cavity Schrödinger cat state preparation uses Ramsey field pulses, enabling the creation of more advanced Schrödinger cat states, but also suffers from losses. Overall, the findings demonstrate the feasibility of preparing Schrödinger cat states in QDCs and atom-cavity systems, providing a more detailed understanding of the preparation process.

Contents

Chapter 1

Introduction

In the last century, the introduction of quantum mechanics has transformed our comprehension of the physical world, unmasking the microscopic realm's quantum nature. The fundamental principles of quantum mechanics involve superposition and entanglement, whereby a quantum system can occupy multiple states simultaneously. Decades after being an object of theoretical interest, quantum superposition has finally emerged as a tool in quantum technology. The concept of superposition was famously illustrated in Erwin Schrödinger's famous thought experiment of a simultaneously alive and dead cat, known as Schrödinger's cat paradox. The experiment results showed that, in quantum mechanics, a system can maintain a superposition of states until it undergoes measurement or observation.

The physical realization of Schrodinger's cat-like superposition has fascinated researchers for years. Schrodinger cat states (SC) are an elegant demonstration of this. These states have the potential to revolutionize quantum computing[15], quantum cryptography[8], and quantum metrology[12]. Over the years, physicists have successfully prospected different systems to create SC states, including vibrational states of a trapped ion[2], propagating photon modes and superconducting qubits.

In this report, we will conduct a comprehensive investigation into preparing Schrödinger cat states. Our study will begin with a review of classical and quantum states; then, we will

inspect Schrodinger cat states and their applications. Finally, we explore the possibilities of engineering these states using different theoretical and numerical protocols.

1.1 Classical and Quantum States

1.1.1 Classical States

Classical mechanics describes the behavior of macroscopic objects, such as billiard balls, cars, and planets. According to classical mechanics, a system's position and momentum define its state. The position of a particle is its location in space, while its momentum is its mass multiplied by its velocity. A particle's state at any time is entirely determined by its location and momentum.

Many types of classical states exist, depending on the specific physical system being studied. Some examples of classical states include:

Stationary states: These states correspond to particles that remain stationary over time, with both their position and momentum remaining constant

Oscillatory states: These states correspond to particles undergoing oscillatory motion, such as simple harmonic motion, with their position and momentum varying periodically over time

Chaotic states: These states correspond to particles that appear to move randomly and erratically, as in chaotic systems like the weather, where the particle's location and momentum change over time without showing any visible pattern.

1.1.2 Quantum States

Quantum mechanics, on the other hand, describes the behavior of microscopic objects at atomic and subatomic levels. Unlike classical mechanics, the quantum realm is inherently probabilistic, introducing the idea of the superposition of states, which means that the system can exist in multiple states simultaneously.

Many quantum states exist, depending on the specific physical system being studied. Some examples of quantum states include:

Coherent states: These are states where the wave function is localized in both position and momentum space and are often used to describe the behavior of systems like lasers.

Entangled states: Another peculiarity of quantum mechanics is quantum entanglement. These states describe the cooperative behavior of two or more quantum systems and cannot be described independently.

Schrödinger cat states: These are a type of quantum state often used to explore the boundary between classical and quantum physics.

1.2 Schrödinger Cat States

1.2.1 Introduction to Schrödinger Cat States

Schrödinger cat states are defined as the quantum superposition of two macroscopically distinct states analogous to the famous thought experiment proposed by Erwin Schrödinger in 1935[16], in which a cat placed in a box is both dead and alive simultaneously. Though in the earlier years, the Preparation of Schrödinger's cat states had attracted research interest as a solution of fundamental quantum physics, now it has emerged as a candidate for quantum computation, quantum communication, and quantum information.

A Schrödinger cat state is a superposition of two coherent states in quantum optics, which are states with well-defined amplitude and phase:

$$\psi = \frac{1}{\sqrt{2}}(|\alpha\rangle + e^{\iota\theta}|-\alpha\rangle) \tag{1.1}$$

Here, $|\alpha\rangle$ is the coherent state with amplitude α, and θ is the relative phase between the two coherent states. The normalization factor ensures an equal chance of identifying the system in any of the two coherent states.

1.2.2 Importance and Potential Applications of Schrödinger Cat States

Schrodinger cat states are anticipated to be a testing ground for the decade-long controversy of quantum measurement. Preparing cat states will imply the controlled study of decoherence; It will contribute to measuring the illusive boundary between the quantum and classical worlds. SC states are beneficial in applied quantum physics and are of fundamental relevance. They promise to be the foundation for quantum computation, cryptography, metrology, and teleportation.

The ability to generate and manipulate Schrödinger cat states has important implications for quantum information processing and technology. One potential application is quantum communication, where Schrödinger cat states can increase the distance over which quantum information can be transmitted. Entangled Schrödinger cat states can send quantum information over long distances without requiring quantum repeaters [4], a possible substitute for entangled photon pairs as quantum channels in quantum teleportation[20]. In quantum sensing and metrology, they are helpful for precision measurements[19]. In addition, Schrödinger cat states can enhance the precision of atomic clocks and other types of sensors. In quantum computing, these states could increase the number of qubits in a quantum computer, leading to greater computational power and the ability to solve problems beyond classical computers' reach.

Chapter 2

Schrödinger cat states in Quantum Dot-Cavity System

Quantum dots are nanoscale semiconductor structures with three-dimensional spatial confinement. Their bandgaps are often called 'zero-dimensional' tunable showing unique electronic and optical properties [10]. The strong interaction between the quantum dot and cavity modes can lead to intriguing phenomena such as vacuum Rabi splitting and entanglement, which are of fundamental importance in quantum optics.

Quantum dots can be precisely engineered and fabricated using advanced semiconductor fabrication techniques. This enables the creation of devices with strictly controlled properties, including their size, shape, and composition. Additionally, quantum dots have long coherence times, making them attractive for quantum information processing and communication applications.

Regarding fundamental advantages, quantum dots offer a unique platform for studying the behavior of electrons in confined systems. These captive systems can simulate the behavior of atoms and molecules, providing a way to study quantum mechanical effects in condensed matter systems. Additionally, the discrete energy levels of quantum dots can be precisely controlled and manipulated, creating complex quantum states that can be used

for various applications.

In recent years the application of Quantum Dots in quantum information processing and quantum communication has dragged attention due to easy on-chip integration. Hence moving different quantum phenomena to solid state-based systems such as QDC systems has attracted researchers.

This study explores two protocols for creating Schrödinger-cat states in a Quantum Dot-Cavity (QDC) system. To accomplish this, we modify already-existing preparation techniques and apply them to the QDC system. The Dot-Driven Protocol (DOD), the first protocol, is based on the idea suggested by Law and Eberly [14]. We rely solely on external laser pulses in the DOD protocol to drive the quantum dot and generate the Schrödinger-cat state. The precise timing of these pulses is crucial to control the interaction between the dot and cavity. The second protocol, the Cavity-Driven Protocol (CAD), is adapted from Banacloche[5] and involves producing a coherent initial state by driving the cavity.

In our analysis of both protocols, we consider the impact of losses and phonon interaction and use realistic parameters verified in current experiments. Our findings show that the DOD protocol suffers from an unfavorable influence of casualties on the sensitive coherence of the Schrödinger cat, leading to the generation of only mixed states under realistic conditions. On the other hand, the CAD protocol shows promise in generating a photonic Schrödinger cat state even under natural conditions. We locate parameter regimes that can be reached experimentally and encourage these states' creation.

In summary, quantum dot-cavity systems offer several advantages for quantum information processing and quantum communication applications. The evolution of Schrodinger cat states in these systems has potential benefits for creating logical qubits and entangled states. The Dot-driven and cavity-driven protocols offer different advantages and can be used to produce Schrodinger cat states in these systems.

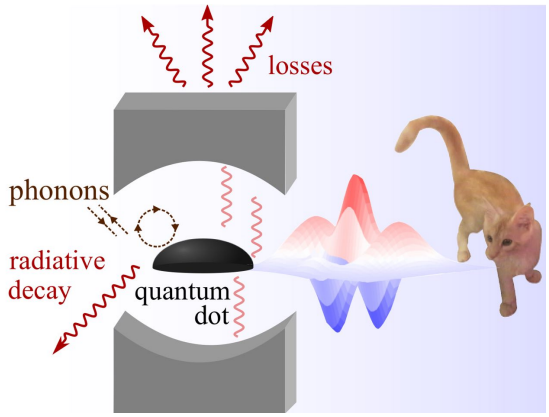

Fig. 2.1 Cat states can be produced on-demand by controlling the emission of photons that occur when QD excitons transition from the conductance band to the valence band [3].

2.1 Theoretical Model

A Quantum Dot Cavity system can be defined by a driven two-level Quantum Dot coupled to a single photon. The Hamiltonian of the system can be written as,

$$\hat{H} = \hat{H}_{QDC} + \hat{H}_{drive} + \hat{H}_{ac-stark} \tag{2.1}$$

From the JC model[18], we characterize QDC Hamiltonian,

$$H_{QDC} = \omega_u |u><u| + \omega_c \hat{a}^\dagger \hat{a} + g_c(\hat{a}\sigma_+ + \hat{a}^\dagger \sigma_-) \tag{2.2}$$

Where $|u\rangle$ is the excited state of energy with energy $\hbar\omega_u$, $\sigma_- = |l\rangle\langle u|$ is the decrement operator for excited state $|u\rangle$ to ground state $|l\rangle$ and $\sigma_+ = |u\rangle\langle l|$ is the increment operator for ground state $|l\rangle$ to excited state $|u\rangle$ and $\breve{a}$ is known as annihilation operator and $\breve{a}^\dagger$ is known as creation operator and coupling between quantum dot and cavity are denoted by g_c. The driving Hamiltonian for DOD protocol can be defined in its general form as follows,

$$\hat{H}_{drive_{DOD}} = -\frac{\hbar}{2}\{f^*_{p_\cdot}(t_\cdot)\sigma_- + f_{p_\cdot}(t_\cdot)\sigma_+\} \tag{2.3}$$

And Driving Hamiltonian for CAD protocol

$$\hat{H}_{drive_{CAD}} = -\frac{\hbar}{2}\{f^*_{p.}(t.)\hat{a} + f_{p.}(t)\hat{a^\dagger}\} \tag{2.4}$$

where the pump field is defined as,

$$f_p(t) = \sum_k f^p_k(t - t_k)e^{-\iota\omega_p(t-t_k)} \tag{2.5}$$

And where $f^p_k(t)$ = Envelope function of the pump fields. and we are going to use Gaussian pulses as pump-field with area $\Theta = 1$

$$f^p_k(t) = \frac{\Theta_i}{\sqrt{2\pi}\sigma}e^{-\frac{t^2}{2\sigma^2}} \tag{2.6}$$

And FWHM of this Gaussian pulse is taken to be $FWHM = 2\sqrt{2\log(2)}\sigma$ with condition $\omega_p = \omega_E$, and in our case, it is nearby 100 fs[3].

To preserve the photonic cat state in the cavity, we have to decouple the quantum dot and cavity, so we apply Ac-Stark pulses and Hamiltonian for ac-stark pulses can be defined as,

$$\hat{H}_{ac-stark} = -\frac{\hbar}{2}\{f^*_{ac-stark}(t.)\sigma_- + f_{ac-stark}(t.)\sigma_+\} \tag{2.7}$$

The rectangular-shaped f_{ac_stark} pulses define the AC-Stark pulses.

$$f_{ac-stark} = e^{-\iota\omega_{A-S}t.}\begin{cases} 0, & t. < -\frac{\tau_{length}}{2} \\ f_s, & -\frac{\tau_{length}}{2} \leq t. \leq \frac{\tau_{length}}{2} \\ 0, & t. > \frac{\tau_{length}}{2} \end{cases} \tag{2.8}$$

The ac-stark pulses are precisely adjusted to remain below the exciton line, with $\omega_{A-S,u} = \omega_{A-S} - \omega_u$, chosen from a range inside the rotating wave approximation.

2.2 Dot Driven Protocol

The Schrödinger's cat state can be expressed in a general form as follows[7],

$$|cat\rangle = N_o^{'}(|\alpha\rangle + e^{i\varphi}|-\alpha\rangle) \tag{2.9}$$

The most prevalent representation of Schrödinger's cat state in Quantum optics involves a normalization constant $N_o^{'}$ and an overall phase φ, and this is our target state via using DOD protocol here; we set $\alpha = \frac{\pi}{2}$ and $\varphi = 0$, and reason of choosing this choice is that it ensures that the related coherent states are differentiable and overall numbers of photons are low enough so we can limit the effects of the cavity losses.

$$|\pi\rangle = N_o^{'}\{|\frac{\pi}{2}\rangle + e^{\iota\varphi}|-\frac{\pi}{2}\rangle\} \tag{2.10}$$

Normalisation constant is,

$$N_o^{'} = \frac{1}{\sqrt{2(1+e^{-\frac{\pi^2}{4}})}} \tag{2.11}$$

In order to produce the desired target state, we will be using the method proposed by C.K. Law and Eberly[14], which was originally proposed to create specific photonic states within an atomic cavity.

2.2.1 Method to Create an Arbitrary Photonic State in a Single Mode Microcavity.

We observe that atom-field interactions can transform the photonic vacuum state into a superposition of Fock states with finite photon numbers, as desired. However, it is important to note that the Hamiltonian imposes a fundamental constraint, limiting the accessibility of certain final states from the initial state.

The Hamiltonian for a system comprising a quantized cavity field interacting with a

driven quantum system is given as follows

$$\hat{H}(t_.) = \omega_c \hat{a}^\dagger \hat{a} + \frac{1}{2}\omega_o \sigma_z + \{r(t_.)e^{-\iota\omega_l t_.} + g(t_.)\hat{a}\}\sigma_+ + \{r(t_.)^* e^{\iota\omega_l t_.} + g(t_.)^* \hat{a}^\dagger\}\sigma_- \tag{2.12}$$

where,ω_l=frequency of driving field, r(t)=coupling strength of atom-external field interaction. g(t)=coupling strength of atom and cavity field interaction. Let the coupling strength of the interaction between the atom and the cavity field be denoted by $g(t_.)$. We will assume that our objective is to prepare a specific photonic state, which will serve as our target state,

$$|\psi_{target}\rangle = \sum_{n=0}^{M} \{C_n|n\rangle\} \tag{2.13}$$

So the atom or trapped ion can make transitions between two levels, so here we have used two interaction channels.

In this setup, we may discriminate between two channels. The first channel represents the atom's interaction with the external driving force. In contrast, the interaction between the atom and the quantized cavity field is related to the second channel. so we have

$$\hat{H}_o = \omega_c \hat{a}^\dagger \hat{a} + \frac{1}{2}\omega_0 \sigma_z \tag{2.14}$$

And,

$$\hat{H}_I = \{r(t_.)e^{-\iota\omega_{L.}t_.} + r^*(t_.)e^{\iota\omega_L t_.}\sigma_-\} + \{g(t_.)\hat{a}\sigma_+ + g^*(t_.)\hat{a}^\dagger\sigma_-\} \tag{2.15}$$

using the unitary operator,

$$U_o = e^{-\iota\hat{H}_o t} \tag{2.16}$$

Then, the wave function is,

$$|\Psi_I\rangle = U^\dagger |\Psi_s\rangle \tag{2.17}$$

and convert the Hamiltonian in interaction picture, with rotating wave approximation on resonance condition ($\omega_L = \omega_o = \omega_c$),

the interaction Hamiltonian (in the interaction picture),

$$\hat{H}_{I_{\cdot}} = \{r(t_{\cdot}) + g(t_{\cdot})\hat{a}\}\sigma_{+} + \{r^{*}(t_{\cdot}) + g^{*}(t_{\cdot})\hat{a}^{\dagger}\sigma_{-}\} \tag{2.18}$$

And we select the initial state (the simplest one),

$$|\Psi(0)\rangle = |0, g\rangle \tag{2.19}$$

Under these conditions, the atom is in its ground state, and the cavity field is in a pure vacuum state, with no excitations present. We presume that both the cavity damping and atomic decay can be neglected. It is worth noting that the highest possible Fock state in the cavity field, denoted by M, depends on the strength of the coupling.
So the strategy of our model is such that we divide total time into 2M equal subintervals with the length of subintervals is $\{\frac{t_{\cdot}}{2\pi} \to \tau_c\}$.
assigning a rule such that only one channel is effective at a time.

$$2(m-1)\tau_c < (t_{\cdot}) < (2m-1)\tau_c, \tag{2.20}$$

$$r(t_{\cdot}) = r_m \quad \& \quad g(t_{\cdot}) = 0 \tag{2.21}$$

$$And, For$$

$$(2m-1)\tau_c < (t_{\cdot}) < (2m)\tau_c, \tag{2.22}$$

$$r(t_{\cdot}) = 0 \quad \& \quad g(t_{\cdot}) = g_m \tag{2.23}$$

The complex constants r_m and g_m (with $1 \leq m \leq M$) must be resolute. The time evolution *öperator* of the system can then be expressed as,

$$U(t^{*}) = Q_M C_M Q_{M-1} C_{M-1} \ldots\ldots\ldots Q_m C_m \ldots\ldots\ldots Q_2 C_2 Q_1 C_1 \tag{2.24}$$

Where $Q'_m s$ are the evolution operator for the g(t) channel and $C'_m s$ are the evolution

operator for r(t) channel then we have,

$$U(t^*) = e^{-\iota H_I t./\hbar} \tag{2.25}$$

$$U(t^*) = e^{-\frac{\iota}{\hbar}(r(t.)+g(t.)\hat{a})\sigma_+ + r^*(t.)+g^*(t.)\check{a}^\dagger)\sigma_-)} \tag{2.26}$$

so for evolution operator for the g(t) channel we define,

$$Q_m = e^{-\frac{\iota}{\hbar}(g_m\hat{a}\sigma_- + g_m^*\hat{a}^\dagger\sigma_+)t} \tag{2.27}$$

And if we solve it, we get the matrix

$$Q_m = \begin{bmatrix} Cos(|g_m|\sqrt{\hat{a}\hat{a}^\dagger}\tau) & \frac{-\iota\hat{a}e^{\iota\phi_m}Sin|g_m|\sqrt{\hat{a}^\dagger\hat{a}}\tau}{\sqrt{\hat{a}^\dagger\hat{a}}} \\ \frac{-\iota\hat{a}^\dagger e^{-\iota\phi_m}Sin|g_m|\sqrt{\hat{a}\hat{a}^\dagger}\tau}{\sqrt{\hat{a}\hat{a}^\dagger}} & Cos(|g_m|\sqrt{\hat{a}^\dagger\hat{a}}\tau) \end{bmatrix} \tag{2.28}$$

and for evolution operator for r(t) channel,

$$C_m = e^{-\frac{\iota}{\hbar}(r(t)\sigma_+ + r^*(t)\sigma_-)t} \tag{2.29}$$

and solving this, we get a matrix,

$$C_m = \begin{bmatrix} Cos(|r_m|\tau) & -\iota e^{\iota\theta_m}Sin(|r_m|\tau) \\ -\iota e^{-\iota\theta_m}Sin(|r_m|\tau) & Cos(|r_m|\tau) \end{bmatrix} \tag{2.30}$$

With, $r_m = |r_m|e^{\iota\theta_m}$,and $g_m = |g_m|e^{\iota\phi_m}$ then,finally to determine the external pulses $(g_m and r_m)$, we use inverse evolution

$$|0, g\rangle = U(-t^*)|n, g\rangle \tag{2.31}$$

And solving this, we get solutions to be like

$$\langle m, g|F_{m+1}\rangle Cos(|g_m\sqrt{m}\tau|) + \iota\langle m-1, e|F_{m+1}\rangle e^{-\iota\phi_m} Sin(|g_m|\sqrt{m}\tau) = 0 \tag{2.32}$$

And

$$\langle m-1, e|Q_m^+|F_{m+1}\rangle Cos(|r_m\tau|) + \iota\langle m-1, g|Q_m^+|F_{m+1}\rangle e^{\iota\phi_m} Sin(|r_m|\tau) = 0 \tag{2.33}$$

Where $|F_m\rangle$ is defined as

$$|F_m\rangle = C_m^\dagger Q_m^\dagger C_{m-1}^\dagger Q_{m-1}^\dagger .....C_1^\dagger Q_1^\dagger |\Psi(t^*)\rangle$$

or,

$$|F_{M+1}\rangle = |\Psi(t^*)\rangle \tag{2.34}$$

And, on solving the above equations, we get relations.

$$tan(|g_m|\sqrt{m}\tau) = \frac{\iota\langle m, g|F_{m+1}\rangle e^{\iota\phi_m}}{\langle m-1|F_{m+1}\rangle} \tag{2.35}$$

and also,

$$tan(|r_m|\tau) = \frac{\iota e^{-\iota\phi_m}\langle m-1, e|Q_m^\dagger|F_{m+1}\rangle}{\langle m-1, g|Q_m^\dagger|F_{m+1}\rangle} \tag{2.36}$$

using these formulas we can get solutions of r_m and g_m.

2.2.2 Implementation in QD

The protocol was initially designed to account for cavity loss channels only. However, to implement it in QDC, the effects of phonons must also be considered. An appropriate laser pulse is required to drive the system using this protocol, and the interaction between the quantum dot and cavity needs to be controlled, which is still challenging. To overcome this challenge, we need to change the magnitude of the quantum dot and cavity coupling while keeping the coupling constant g_c constant. During the driving of the field,

the quantum dot and cavity need to be decoupled, which can be achieved by using Ac-Stark pulses. Alternatively, we can avoid decoupling altogether to achieve our goal with shorter pulses. It is crucial to consider that switching off the laser takes more time than the system's dynamics. Therefore, we need to switch off the laser with precise timing to ensure that the quantum dot and cavity remain coupled. We can use a Gaussian pulse with the same area as the rectangular pulse to drive the system. The FWHM of the Gaussian pulse can be set to 100 fs.

Fig. 2.2 Series of pulses for DOD protocol where at t_c pulses are on peak and Θ is the area of applied pulse[3]

Number of the pulse	t_c (ps)	Θ (π)
1	0.1	-1
2	14.2	-1
3	24.1	-1
4	34.6	1
5	40.0	-1
6	46.5	-1
7	53.7	-1
8	60.7	-1
9	67.2	-1
10	72.1	-1

2.2.3 The ideal case

Figure(2.3) shows the dynamics of the Quantum Dot Cavity in a dot-driven protocol where the bottommost panel shows ten series of pluses to prepare the Schrödinger's cat state of equation (2.7), and this pulse sequence is derived from equations (2.33) and (2.34) and here, we are applying 10-π pulses with arc area $\Theta = 1$. The time distinction between two consecutive pulses is time τ_i where the cavity coupling constant $\mathbf{g}$(constant) takes effect. After reaching the desired state, the coupling between the quantum dot and cavity should be off to maintain the generated Schrödinger's cat state in the hole, and the result of this time evolution can be seen in the second bottommost panel that photons are partially created after every pulse means double bottom-most panel shows exciton occupation n_X in the cavity, and then average numbers photon $\langle n \rangle$ inside the cavity is shown in 2^{nd} upper panel and it amplify after each pulse. To know whether we have

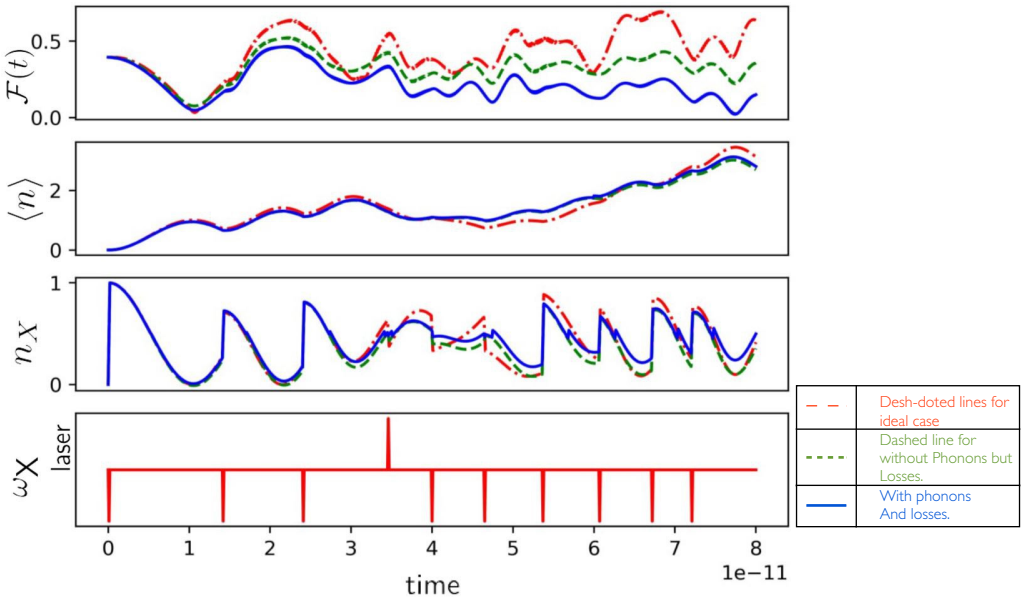

Fig. 2.3 These plots visualize the system's dynamics in DOD protocol in the ideal case. Where bottom most panels show an external pulse, then the Second panel from the bottom shows exciton occupation n_E then the second from the top shows the average number of photons $\langle n \rangle$, then top most panel shows time-dependent fidelity[11],[1].

generated a Schrödinger's cat state in this process, We examine the consistency between the target and end states. A measure of how closely or similarly two different states are is called fidelity.

For Mixed state fidelity is defined as,

$$F(\rho_1, \rho_2) = [Tr\sqrt{\sqrt{\rho_1}\rho_2\sqrt{\rho_1}}]^2 \tag{2.37}$$

Some properties of fidelity are[13],

$$0 \leq F(\rho_1, \rho_2) \leq l \tag{2.38}$$

$F(\rho_1, \rho_2)$=1 if and only if $\rho_1 = \rho_2$,i.e. if the states are exactly similar.

$$F(\rho_1, \rho_2) = F(\rho_2, \rho_1) \tag{2.39}$$

$\rho = |\Phi >< \Phi|$, is for a pure state the,

$$F(\rho_1, \rho_2) = \langle \Phi | \rho_2 | \Phi \rangle = trace(\rho_1 \rho_2) \tag{2.40}$$

where, ρ_1 =density matrix of target state and ρ_2 = density matrix of $H_{dynamics}$[13]. And, in the plot, we get that the fidelity approaches one after the 10^{nth} pulse. That result shows that with this protocol, in the ideal case where we have ignored any losses and phonon effects, we can generate a cat state, which can also be confirmed by analyzing the Wigner function. And this Wigner function is defined as[17],

$$W(\vartheta) = \frac{1}{\pi^2} \int d^2\alpha C_{Wely}(\alpha) e^{-(\alpha\vartheta^\dagger - \alpha^\dagger \vartheta)} \tag{2.41}$$

With, $C_{Wely}(\alpha)$ defined as Weyl ordered characteristic function and $C_{Wely}(\alpha)$ defined as "$tarce[\rho D(\alpha)]$" and $D(\alpha)$ is the displacement vector,

$$\vec{D}(\alpha) = e^{-\frac{|\alpha|^2}{2}} e^{\alpha \hat{a}^\dagger} e^{-\alpha \check{a}} \tag{2.42}$$

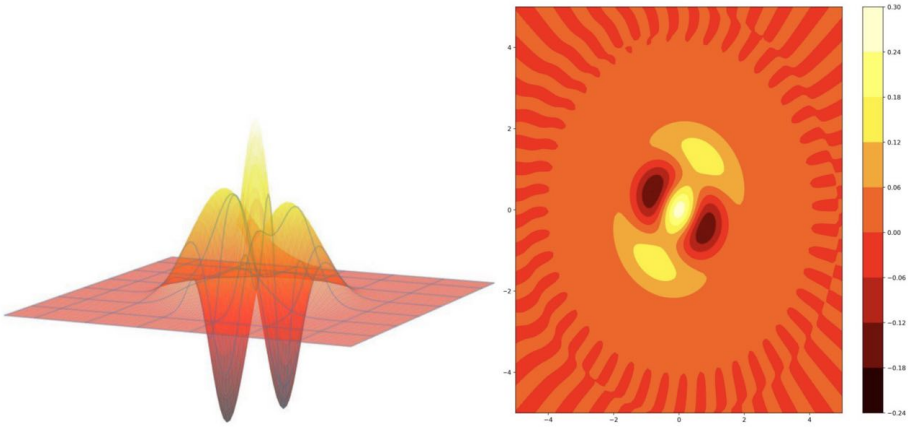

Fig. 2.4 Under ideal circumstances, the Wigner functions for the photonic state produced by the DOD procedure[11],[1]

This figure shows all Schrödinger's cat state features, where two Gaussian curves show two macroscopically recognizable forms. These coherent states oscillate around the center point, which shows their superposition characteristics.

And non-classicality is an essential property of Schrödinger's cat state, and non-classicality is shown by δ. The negative part of the Wigner function is related to the nonclassical nature of the states, and the positive value indicates classical nature. And we can calculate the non-classicality δ by using the form,

$$\delta = \frac{\int[|W(\frac{\pi}{2})| - W(\frac{\pi}{2})]d(\frac{\pi}{2})}{\int W(\frac{\pi}{2})d(\frac{\pi}{2})} \tag{2.43}$$

Non-classicality denotes the quantum nature of the Wigner function, and $\delta = 0$ means we are in a classical state. For DOD protocol in the ideal case, we obtain $\delta = 0.51$. So adoption of the protocol to generate Schrödinger's cat state is quite successful.

2.2.4 Loss and phonons effects.

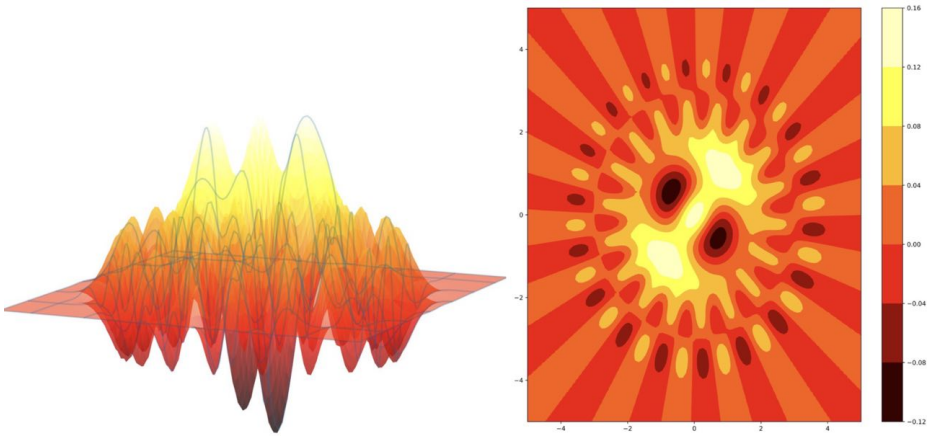

Fig. 2.5 The Wigner functions for the photonic state evolved by the $D\ddot{O}D$ procedure with cavity losses and other possible losses that occur in the atomic system[11],[1]

Now, we see the loss channels. First, we consider loss channels due to radiative decay(due to recombination of exciton) of quantum dot and cavity losses (Here, we believe that our cavity is imperfect, and the cavity mode can lose photons). Then we will see fidelity drops to $F = 48.7\%$, and the non-classicality measure reduces to $\delta = 0.03$. This Wigner function figure demonstrates that the domains of the Wigner function's negative values have all but vanished. Now consider loss channels as well as phonons. These phonons will

destroy the remaining non-classicality. And the fidelity drops to $F = 25\%$, and non-classicality measures reduce to $\delta = 0$, which shows a pure classical state.

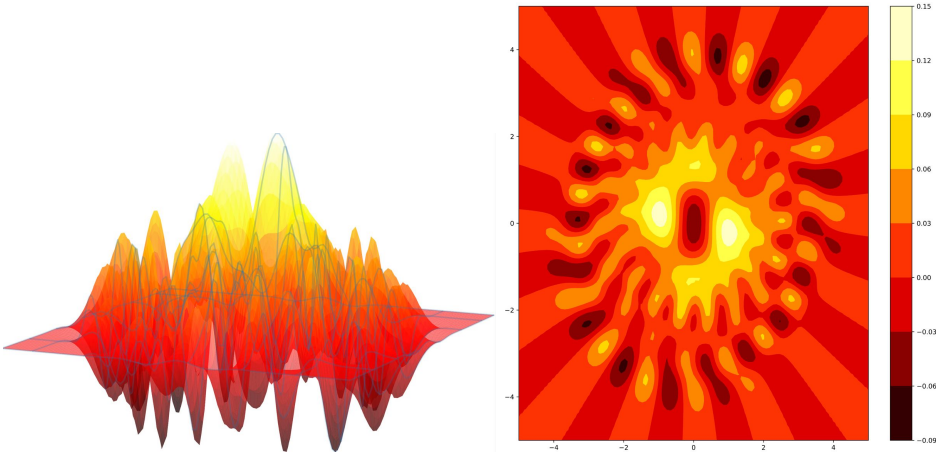

Fig. 2.6 The Wigner functions for the photonic state generated by the DOD procedure with both decay cavity loss and phonon loss[11],[1]

.

From all analysis, it is clear that fidelity is insufficient to define a state's actual nature, and it is necessary to consider non-classicality parameters like δ simultaneously. So overall, the DOD protocol can create Schrödinger's cat state only in ideal conditions. In realistic cases, the cat state cannot survive the environmental coupling even at cryogenic temperature(4K), and the phonon effect destroy the coherence between coherent stats.

2.3 Cavity Driven Protocol

The Collapsed And Revival (CAD) protocol is based on a method proposed by Julio Gea-Banacloche[5], which uncovered two remarkable features of the collapse-and-revival phenomenon in the JCM: (1) the QD and photonic subspaces become distinct at half the revival time, and (2) a Schrödinger-cat state is produced in the cavity mode.
To generate a Schrödinger-cat state using the CAD protocol, it is crucial to begin with; the starting state of the Jaynes-Cummings dynamics is a coherent state in the cavity mode. At half the rebirth time, the system produces a photonic state, which is created in the following manner:

$$|\Psi\rangle = N(|\phi_+\rangle + |\phi_-\rangle) \tag{2.44}$$

$$Where,$$

$$|\phi_\pm\rangle = \exp^{-\frac{1}{2}\langle\eta\rangle} \sum_{\eta=0}^{\infty} \frac{\langle\eta\rangle^{\frac{\eta}{2}}}{\sqrt{\eta!}} \exp^{-\iota\eta\phi} \exp^{\mp\iota\pi\sqrt{\langle\eta\rangle\eta}} |\eta\rangle \tag{2.45}$$

Equation (2.45) presents a different form of a Schrödinger cat state, where the normalization constant N ensures. The mean photon count of the initial coherent state is denoted by $\langle\eta\rangle = |\alpha|^2$, and the phase ϕ is determined by a short analytical calculation to be $3\pi/2$ in the case of an actual envelope Gaussian pulse. It should be noted that these states are macroscopically recognizable but are not coherent states like those in Eq. (2.7) due to the presence of a phase that depends on both $\langle\eta\rangle$and n in Eq. (2.46).
To achieve our goal of generating the target state, we employ the state preparation method proposed by Julio Gea-Banacloche[5], which involves using a Quantum Apparatus.

2.3.1 Wavefunction Collapse and Quantum Revivals in the Jaynes-Cummings Model

The Jaynes-Cummings model (JCM)[18] is a fascinating quantum system that depicts the interaction between a two-level atom and a single mode of the electromagnetic radiation field. This model has garnered significant attention due to its exact solvability and recent experimental verification. The JCM displays remarkable and unexpected dynamics that diverge significantly from the semiclassical theory. A central and fundamental inquiry addressed in this model is whether it is feasible to portray the evolution of an interacting quantum system by a unitary state vector, primarily in the presence of entanglement between the atom and the field. Entanglement plays an indispensable and essential role in JCM dynamics and is a critical component of various proposals related to measurement theory. Consequently, entanglement has been the subject of numerous and extensive theoretical investigations in the condition of the JCM.

And interaction Hamiltonian in the JCM model can be written as

$$\hat{H}_I = g_c\{|\uparrow\rangle\langle\downarrow|\hat{a} + |\downarrow\rangle\langle\uparrow|\hat{a}^\dagger\} \tag{2.46}$$

Assuming $|\uparrow\rangle$ represents the upper state, $|\downarrow\rangle$ represents the lower state, and $\check{a}$ and $\check{a}^\dagger$ denote the annihilation and creation operators, respectively, while g_c is the coupling constant, the interaction Hamiltonian in the interaction picture can be expressed as follows

$$\hat{V}_I = g_c\{|\uparrow\rangle\langle\downarrow|\hat{a}e^{\iota\Lambda t.} + |\downarrow\rangle\langle\uparrow|\hat{a}^\dagger e^{-\iota\Lambda t.}\} \tag{2.47}$$

With, $\Lambda = \omega - \nu$ is, de-escalation between fields.

And the solution of the Schrödinger equation for the primary state of the atom and field

is given as,

$$|\varphi(0)\rangle_A = \alpha|\uparrow\rangle + \beta|\downarrow\rangle \tag{2.48}$$

And,

$$|\varphi(0)\rangle_{CF} = \sum_{\eta=0}^{\infty} C_\eta|\eta\rangle \tag{2.49}$$

The well-known answer for the JC model at any given time t is then provided by,

$$|\Psi(t_.)\rangle = \sum_\eta \{C_{\uparrow,\eta}|\uparrow,\eta\rangle + C_{\downarrow,\eta}|\downarrow,\eta\rangle\} \tag{2.50}$$

$$|\Psi(t_.)\rangle = \sum \{\{\alpha C_\eta cos(g_c t_. \sqrt{\eta+1}) - \iota\beta C_{\eta+1} sin(g_c\sqrt{\eta+1}t_.)\}|\uparrow\rangle$$

$$+ \{\text{-}\iota\alpha C_{\eta-1} sin(g_c t_.\sqrt{\eta}) + \beta C_\eta cos(g_c t_.\sqrt{\eta})\}|\downarrow\rangle\} \tag{2.51}$$

From the Schrödinger equation, we get solutions to be like as,

$$\dot{C}_{\uparrow,\eta} = -\iota g_c\sqrt{\eta+1} e^{\iota\Lambda t_.} C_{\downarrow,\eta+1} \tag{2.52}$$

$$\dot{C}_{\downarrow,\eta+1} = -\iota g_c\sqrt{\eta+1} e^{-\iota\Lambda t_.} C_{\uparrow,\eta} \tag{2.53}$$

After evaluating the eq.(2.52) and (2.53), we get

$$C_{\uparrow,\eta}(t_.) = C_\eta(0)\{cos(\frac{\Omega_\eta t_.}{2}) - \frac{\iota\Lambda}{\Omega_\eta} sin(\frac{\Omega_\eta t_.}{2})\} e^{\frac{\iota\Lambda t_.}{2}} \tag{2.54}$$

$$C_{\downarrow,\eta+1}(t_.) = -C_\eta(0)\frac{2\iota g_c\sqrt{\eta+1}}{\Omega_\eta} sin(\frac{\Omega_\eta t_.}{2}) e^{-\frac{\iota\Lambda t_.}{2}} \tag{2.55}$$

Now, the evaluate the Wigner function,

$$W(t_.) = \langle\varphi_\uparrow|\varphi_\uparrow\rangle - \langle\varphi_\downarrow|\varphi_\downarrow\rangle \tag{2.56}$$

The atomic inversion's behavior reveals the ion's current state of motion.

$$W(t_.) = \sum_{\eta=0}^{\infty} |C_\eta(0)|^2 \frac{\lambda^2}{\Omega_\eta^2} + |C_\eta(0)|^2 \frac{4g_c^2(\eta+1)}{\Omega_\eta^2}\{cos^2(\frac{\Omega_\eta t_.}{2}) - sin^2(\frac{\Omega_\eta t_.}{2})\} \tag{2.57}$$

$$W(t_.) = \sum_{=0}^{\infty} \rho_{\eta\eta}(0)\{\frac{\Lambda^2}{\Omega_\eta^2} + \frac{4g_c^2(\eta+1)}{\Omega_\eta^2}\{cos(\Omega_\eta t_.)\}\} \tag{2.58}$$

From eq(2.51), it is clear that the atom and the cavity field are entangled. Now that the density matrix formalism has been introduced, it may be used to represent the development of atoms alone.

$$\rho_A = Tr_{CF}(|\psi(t_.)\rangle\langle\psi(t_.)|) \tag{2.59}$$

This density matrix does not describe a single atom but an ensemble of identically prepared atoms. The state for the ensemble to be in a pure state,

$$Tr(\rho_A)^2 = 1 \tag{2.60}$$

And for statistical mixture,

$$Tr(\rho_A)^2 = 1/2 \tag{2.61}$$

In equation (2.58), we observe the state vector's collapse and revival. The plot in the figure above shows the time evolution of $Tr(\rho_A^2)$, where $\bar{\eta} = 49$, and the atom is primarily in the lower state. The atomic state remains pure during a short time interval of $\frac{1}{g_c}$. The collapse time, when the atomic inversion occurs, is also visible. At this point, $Tr(\rho_A^2)$ collapses to a value of 1/2, indicating that the ensemble is in a mixed state. At $t_0 = \bar{\eta}^{-\frac{1}{2}}\pi/g_c$, $Tr(\rho_A^2) = 1$ again, and the atom is once again in a pure state, We see that this rebirth takes place right within the collapse region where the atomic inversion is still zero. Hence, Looking upon the atomic inversion, the conventional revival is $t_{rev} = 2\pi g_c \bar{\eta}^{\frac{1}{2}}$

so $t_0 = t_{rev}/2$.

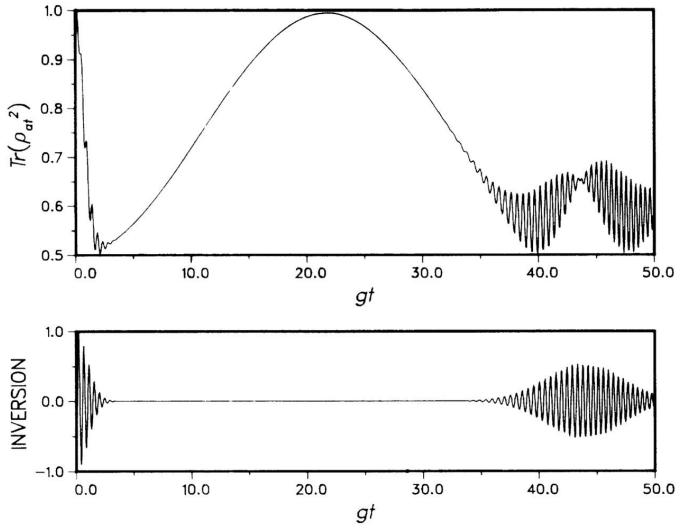

Fig. 2.7 The time evolution of $Tr(\rho_A^2(t_.))$ and atomic inversion at $\bar{\eta} = 49$[5].

And using binomial expansion, we can write,

$$g_c t_.(\eta+1)^{1/2} = g_c t_. \eta^{1/2} + \frac{\pi}{2} \tag{2.62}$$

Putting(2.62) in equation(2.51) and C_η=$e^{-\iota\phi}C_{\eta-1}$, $|\Phi(t_.)\rangle$,we get,

$$|\Phi(t_.)\rangle = \sum(\{\{\alpha C_\eta cos(g_c\sqrt{\eta+1}t_.) - \iota\beta C_{\eta+1} sin(g_.\sqrt{\eta+1}t_.)\}|\uparrow\rangle + \{-\iota\alpha C_{\eta-1} sin(g_c)\}|\downarrow\rangle\}|\eta\rangle \tag{2.63}$$

$$|\Phi(t_.)\rangle = \sum\{\{\alpha e^{-\iota\phi} C_{\eta-1} cos(g_c\sqrt{\eta}t_. + \pi/2) - \iota\beta C_{\eta+1} sin(g_c\sqrt{\eta}t_. + \pi/2)\}|\uparrow\rangle$$
$$+\{-\iota\alpha C_{\eta-1} sin(g_c\sqrt{\eta}t_.) + \beta C_\eta cos(g_c\sqrt{\eta}t_.)\}|\downarrow\rangle\}|\eta\rangle \tag{2.64}$$

$$|\Phi(t_.)\rangle = \{\sum \alpha C_{\eta-1} sin(g_c\sqrt{\eta}t_.)\{e^{-\iota\phi}|\uparrow\rangle + \iota|\downarrow\rangle\} + \beta C_\eta cos(g_c\sqrt{\eta}t_.)\{e^{-\iota\phi}|\uparrow\rangle + \iota|\downarrow\rangle\}\}|\eta\rangle \tag{2.65}$$

$$|\Phi(t_.)\rangle = \{e^{-\iota\phi}|\uparrow\rangle + \iota|\downarrow\rangle\}\{\sum \alpha C_{\eta-1} sin(g_c\sqrt{\eta}t_.) + \iota\beta C_\eta cos(g_c\sqrt{\eta}t_.)\}|\eta\rangle \tag{2.66}$$

There is no link between the states. Thus, they are in a condition of purity,

$$|\Psi(t_. \approx t_o)\rangle = \frac{1}{\sqrt{2}}\{e^{-\iota\phi}|\uparrow\rangle + \iota|\downarrow\rangle\} \tag{2.67}$$

This is an impressive outcome because we obtained this state $|\Psi(t_. \approx t_o)\rangle$ irrespective of the initial state's properties leading up to this point.

$$|\Psi_\pm\rangle = \frac{1}{\sqrt{2}}\{e^{-\iota\phi}|\uparrow\rangle \pm \iota|\downarrow\rangle\} \tag{2.68}$$

As far as $g_c t_./\bar{\eta}$ is within a reasonable range, the state continues to evolve into a pure state instead of collapsing.

$$|\Psi_\pm\rangle = \frac{1}{\sqrt{2}}(e^{-\iota\phi}|\uparrow> \pm e^{\pm\iota g_c t_./2\bar{\eta}^{1/2}}|\downarrow\rangle) \tag{2.69}$$

By including the field component of ψ,

$$|\psi(0)_{CF}\rangle = \sum_{n\eta=0}^{\infty} C_\eta|\eta\rangle \tag{2.70}$$

$$|\psi\rangle = \frac{1}{\sqrt{2}}(e^{-\iota\phi}|\uparrow\rangle \pm e^{\pm\iota g_c t_./2\bar{\eta}^{1/2}}|\downarrow\rangle)\sum_{\eta=0}^{\infty} e^{\pm\iota g_c t_./2\bar{\eta}^{1/2}} C_\eta|\eta\rangle \tag{2.71}$$

Now we can substitute, $C_\eta = e^{-\bar{\eta}/2}\sum_{\eta=0}^{\infty}\frac{\bar{\eta}^\eta}{\sqrt{\eta!}}e^{-\iota\eta\phi}$

$$|\psi\rangle = \frac{1}{\sqrt{2}}(e^{-\iota\phi}|\uparrow\rangle \pm e^{\pm\iota g_c t_./2\bar{\eta}^{1/2}}|\downarrow\rangle)\sum_{\eta=0}^{\infty} e^{\pm\iota g_c t_./2\bar{\eta}^{1/2}} e^{-\bar{\eta}/2}\frac{\bar{\eta}^\eta}{\sqrt{\eta!}}e^{-\iota\eta\phi}|\eta\rangle \tag{2.72}$$

$$|\psi\rangle = \frac{1}{\sqrt{2}}(e^{-\iota\phi}|\uparrow\rangle \pm e^{\pm\iota g_c t_./2\bar{\eta}^{1/2}}|\downarrow\rangle)|\Phi_+\rangle + \frac{1}{\sqrt{2}}(e^{-\iota\phi}|\uparrow\rangle \pm e^{\pm\iota g_c t_,/2\bar{\eta}^{1/2}}|\downarrow\rangle)|\Phi_-\rangle \tag{2.73}$$

Where,

$$|\Phi_\pm\rangle = \sum_{\eta=0}^{\infty} e^{\pm\iota g_c t_./2\bar{\eta}^{1/2}} e^{-\iota\eta\phi}|\eta\rangle \tag{2.74}$$

When $t_{\cdot} = t_0$, the two atomic states in the equation become identical, and a Schrodinger cat state is formed as a linear combination of $|\Phi_{\pm}(t_0)\rangle$. This state represents two microscopically distinct field states.

2.3.2 Improvising this protocol in QDC in CAD protocol

Ideal case

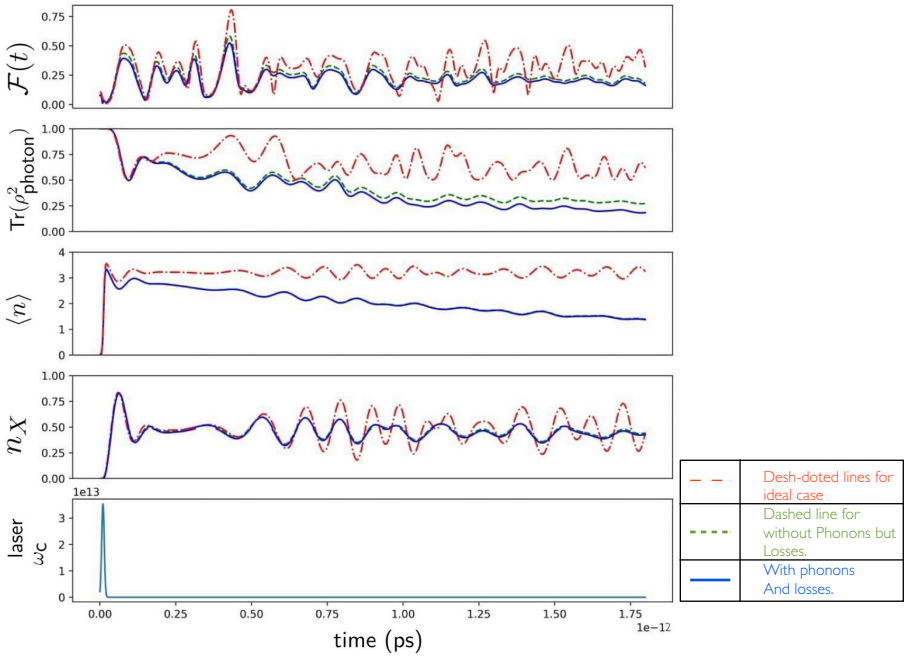

Fig. 2.8 The plot displays the dynamics of the quantum dot cavity system in the CAD method, from bottom to top: the laser pulse that excites the system, the exciton occupation number n_X, the average photon number $\langle n \rangle$, $Tr(\rho^2)$, and finally the fidelity[11],[1].

Figure (2.7) showcases the remarkable QDC dynamics in the cavity-driven mode with a pulse area of 1.2π. The dotted lines show the ideal case. For $\bar{n} = (\Theta/2)^2$, the mean photon number is approximately 3, which is not enough to generate differentiable collapse and revival behaviors. However, the exciton dynamics suggest a revival around 80 ps. The value of tr(photonic density matrix)^2 is almost unity, indicating that the photonic subsystem is near to a pure state. The fidelity Oscillates in a bell-shaped envelope and reaches a peak of 88.1% 42.9 ps after the pulse. To preserve the cat state's integrity, a

supplementary driving pulse must decouple the quantum dot from the cavity. Figure(2.8)

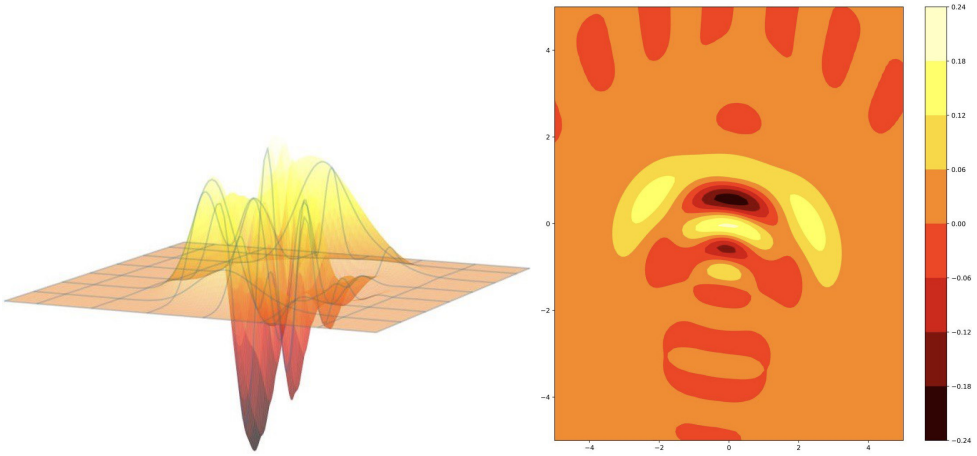

Fig. 2.9 Dynamics of Wigner function in CAD protocol in the ideal case[11],[1].

portrays the Wigner function at maximum fidelity during decoupling, where oscillations between negative values among the two elongated Gaussians imply a coherent state. Schrodinger cat state, to be precise. Notably, this protocol's efficacy hinges on the pulse area. Fidelity increases as $\bar{\eta} \to 0$ and displays oscillatory behavior for higher $\bar{\eta}$. For decreasing $\bar{\eta}$, commitment approaches unity while decreases. Therefore, low $\bar{n}$ states are unsuitable as a *Schrödinger* cat state. And if we apply the limit $\langle n \rangle \to \infty$, the equation (2.68) can be modified as.

$$|\Phi\rangle \to e^{\mp \iota \bar{n} \pi/2} | \mp \iota \alpha \rangle \tag{2.75}$$

2.3.3 Loss and Phonon effect

Cavity losses and radiative decay severely impact the creation of *Schrödinger* cat states using the CAD protocol, as evidenced by Figure(2.7). The adverse effects are powerful for high photon number states, denoted by $\bar{\eta}$. The fidelity is reduced to zero due to the proportional increase in effective loss rates with higher Fock states. Furthermore, exceeding the ideal pulse duration of 1.5 results in the non-classicality measure δ becoming zero, thereby preventing the generation of Schrodinger cat states under such

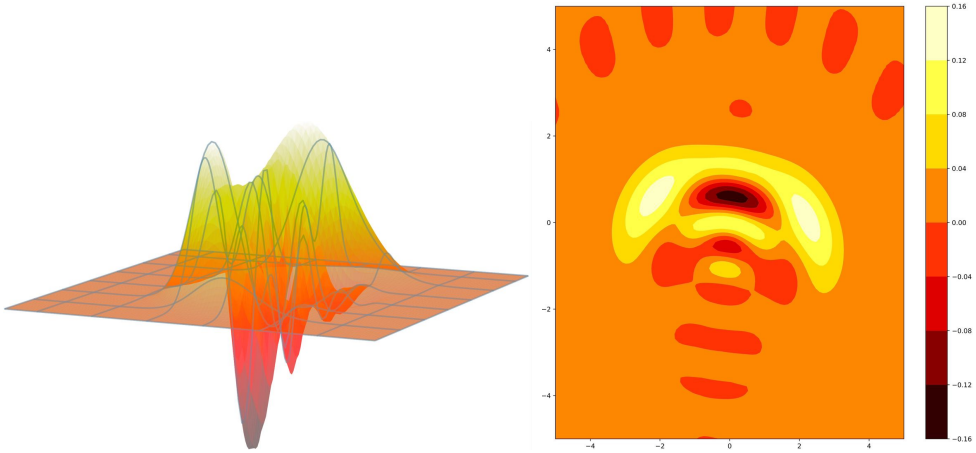

Fig. 2.10 Dynamics of Wigner function in CAD protocol with the presence of decay and cavity losses[11],[1].

conditions. In the limit of $\bar{\eta}$ approaching infinity, there is a complete absence of Schrodinger cat states. Therefore, it is crucial to carefully consider and mitigate the effect of cavity losses and radiative decay in preparing Schrodinger cat states using the CAD protocol. These findings underscore the need for innovative techniques and robust experimental designs to minimize the effects of unwanted decoherence in quantum systems. When accounting for the impact of phonons and loss effects, the dynamics of a

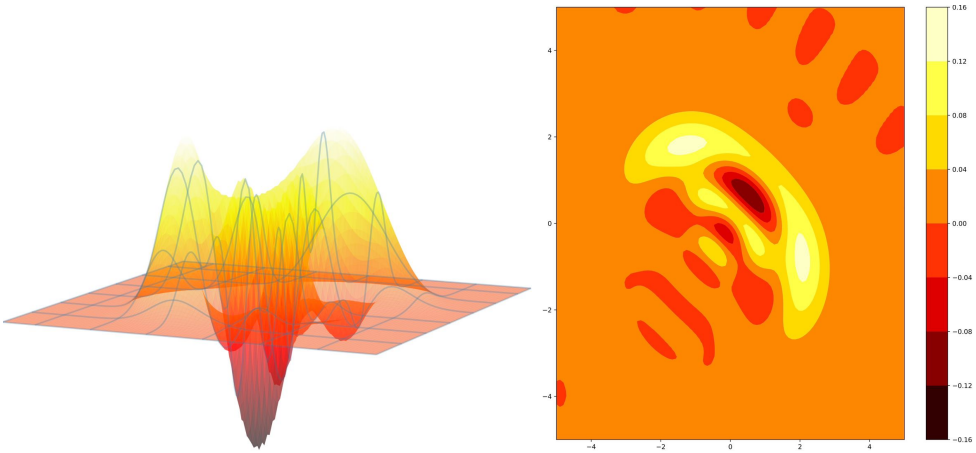

Fig. 2.11 Dynamics of Wigner function in CAD protocol with both decay cavity loss and phonon loss[11],[1].

quantum system are further smoothed out, resulting in a decrease in non-classicality and fidelity of the state. This effect is observed even considering only the impact of losses

without phonons. It is important to note that the specific parameters that dictate these findings, such as temperature and QD geometry, are crucial to preparing a Schrodinger cat state. However, it is essential to emphasize that the loss effects significantly impact the preparation of such a state. Loss effects and phonons can dramatically impact a quantum system's behavior and must be carefully considered in any design or analysis.

Chapter 3

Schrödinger Cat States in Atom-Cavity system

The atom-cavity system is an up-and-coming platform for exploring the quantum behavior of physical systems. Confining an atom within a high-Quality optical cavity makes creating a strong interaction between the atom and the cavity field possible, leading to various quantum phenomena. One of the most intriguing phenomena is the generation of Schrödinger Cat states, which are highly nonclassical states that exhibit properties of waves and particles.

The ability to generate Schrödinger Cat states in the atom-cavity system holds enormous potential benefits. Firstly, these states have been proposed as a resource for quantum information processing, offering the possibility of performing impossible tasks with classical systems. Secondly, they provide a new regime for testing the foundations of quantum mechanics and exploring the boundary between the quantum and classical worlds.

However, the generation of Schrödinger Cat states in the atom-cavity system has challenges. One major challenge is the effect of decoherence, which can quickly destroy the delicate quantum superpositions required for creating these states. Additionally, the

preparation and measurement of these states require exact control over the atom and cavity field, which poses another significant challenge.

In addition to these theoretical and experimental challenges, physical world difficulties also arise in generating Schrödinger Cat states in the atom-cavity system. External noise sources, such as temperature and magnetic field fluctuations, can significantly disrupt the delicate quantum coherence required for creating these states. Furthermore, imperfections in the cavity and atoms, such as losses and defects, can limit the efficiency and fidelity of the state preparation and measurement processes.

To overcome these challenges, sophisticated techniques for controlling and manipulating the atom and cavity field are required, along with careful engineering of the experimental setup to minimize external noise sources and imperfections. Despite these challenges, the potential benefits of generating Schrödinger Cat states in the atom-cavity system make it an up-and-coming area of research in quantum physics. The following chapter will discuss one of the techniques[9] and, using the simulation, will discuss physical world difficulties and generate Schrödinger Cat states in the atom-cavity system.

3.1 Generating Nonclassical Atom-Light States via Deterministic Entanglement

Using coherent laser pulses in this technique, In an optical cavity containing only one confined atom, it is possible to construct entangled light-matter Schrödinger cat states with certainty. The Atom is placed in a superposition of two spin states, and the resulting Entanglement is utilized to manipulate the flying optical cat state. This is accomplished through a coherent rotation followed by analysis of the atomic spin direction, which can be performed despite the atom and light being widely separated[9].

3.1.1 Protocol

In this scheme, the focus is on an atom with three appropriate energy levels that are confined within an optical cavity. Specifically, the ground-state manifold of the atom contains levels $|0\rangle$ and $|1\rangle$, which have different hyperfine spins. In contrast, level $|e\rangle$ is an excited state that can be reached from level $|1\rangle$ through resonant coupling to a cavity mode ac. The input optical pulse, generated in a weak coherent state $|\alpha\rangle$, is also resonantly driven by this cavity mode ac. The atom-cavity field interaction is, therefore, a dispersive one described by the effective interaction Hamiltonian

$$\hat{H}_I = g_c \hat{a}^\dagger \hat{a} \sigma_z \tag{3.1}$$

Where g_c is the coupling constant,$\breve{a}$ is the annihilation *operatör*, and σ_z is the Pauli matrix along the z-direction. Suppose the atom is initially in level $|0\rangle$. In that case, the input pulse will resonate with the bare cavity mode ac after resonant reflection, resulting in a phase shift of $e^{\iota\phi}$, as expected from standard quantum optics calculations. This causes the practical state of the pulse to become $|-\alpha\rangle$. However, suppose the atom is prepared in level $|1\rangle$. In that case, the frequency of the dressed cavity mode is significantly detuned from the center frequency of the input pulse due to the strong atom-cavity interaction. Therefore, the interaction between the atom-cavity system and the input pulse does not play an important role. The reflection is similar to a mirror, preserving the pulse shape and phase. As long as the amplitude of the input pulse, denoted by α, is not too large, the pulse will remain in the same state $|\alpha\rangle$ after the reflection. However, outside the cavity on either side - in regions are referred to as

Ramsey zones. And here, Ramsey zones are set to produce $\pi/2$ pulse,

$$|e\rangle \rightarrow \frac{1}{\sqrt{2}}(|1\rangle + |0\rangle) \tag{3.2}$$

$$|g\rangle \rightarrow \frac{1}{\sqrt{2}}(|0\rangle - |1\rangle) \tag{3.3}$$

To generate a Schrödinger-cat state, the trapped atom is prepared in a superposition

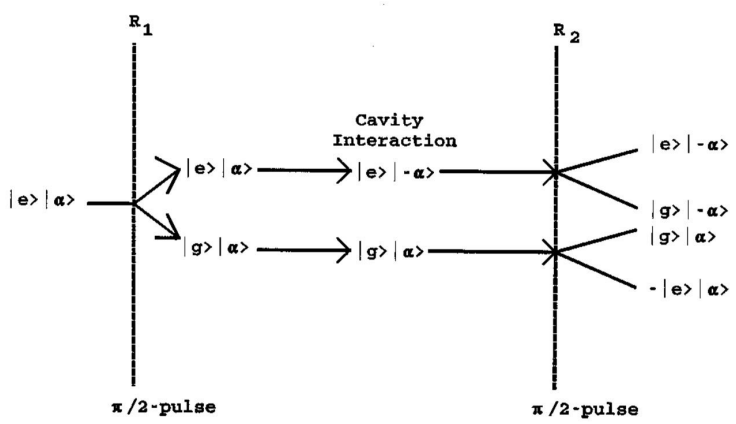

Fig. 3.1 Disruptive small pathways within the system resulting from Ramsey microwave interaction in R1 and R2 zones and cavity interaction in the center of the diagram, indicating potential outcomes[6].

state of $(|0\rangle + |1\rangle)/(\sqrt{2})$, and a coherent pulse $|\alpha\rangle$ is reflected with this single-atom cavity.The initial state of the atom-cavity field system is $|\Psi_{AF}(0)\rangle = |\Psi_A\rangle|\alpha\rangle$ .With an atom in the cavity, at time t, the system state vector is,

$$|\Psi_{AF}(t)\rangle = e^{-\iota \hat{H}_I t/\hbar}|\Psi_F(0)\rangle \tag{3.4}$$

And we get,

$$|\Psi_{AF}(t)\rangle = \frac{1}{\sqrt{2}}(|1\rangle|\alpha e^{\iota g t}\rangle + |0\rangle|\alpha\rangle) \tag{3.5}$$

We now suppose that the atomic velocity is selected such that, at the time, the atom leaves the cavity gt=π. Then our state vector has the form

$$|\Psi(\frac{g}{\pi})\rangle_{AF} = \frac{1}{\sqrt{2}}\{|1\rangle(|-\alpha\rangle) + |0\rangle(|\alpha\rangle)\} \tag{3.6}$$

To Obtain superposition of the $|\alpha\rangle$ and $|-\alpha\rangle$ we must apply the second Ramsey field pulse

$$|\Psi(\frac{g}{\pi})\rangle_{AF} \rightarrow |\Psi'(\frac{g}{\pi})\rangle_{AF} \tag{3.7}$$

$$|\Psi(\frac{g}{\pi})\rangle_{AF} = \frac{1}{2}\{|1\rangle(|\alpha\rangle - |-\alpha\rangle) + |0\rangle(|\alpha\rangle + |-\alpha\rangle)\} \tag{3.8}$$

Now,selecively ionzing and detecting $|0\rangle$ projects the cavity field in the state $|\Phi_e\rangle = N_e(|\alpha\rangle + |-\alpha\rangle)$, while for $|e\rangle$ into $|\Phi_0\rangle = N_o(|\alpha\rangle - |-\alpha\rangle)$,Where $|\Phi_e\rangle$ is defined as even cat state and$|\Phi_0\rangle$ is defined as odd cat state.

3.1.2 Results

We have discerned Wigner functions that showcase two Gaussian peaks and interference fringes at the center, indicative of the coherent superposition state. Notably, the even cat state shows a local maximum, and the odd cat state demonstrates a local minimum at the center of the Wigner distribution. The fidelities of these measured states with their ideal counterparts (even and odd cat states) are a respectable 0.78 and 0.67, respectively, cementing their dependable approximation to the ideal states. Additionally, the enigmatic character of cat states - the presence of hostile regions in the Wigner function - remains unexplainable by classical means.

In an atom-cavity system, the impact of dissipation on state preparation can significantly affect the fidelity of the prepared state. In our study, we investigated the preparation of even and odd cat states with environmental coupling and found that in the ideal case, the fidelity for even cat states was 0.78, and for odd cat states, it was 0.67. However, when

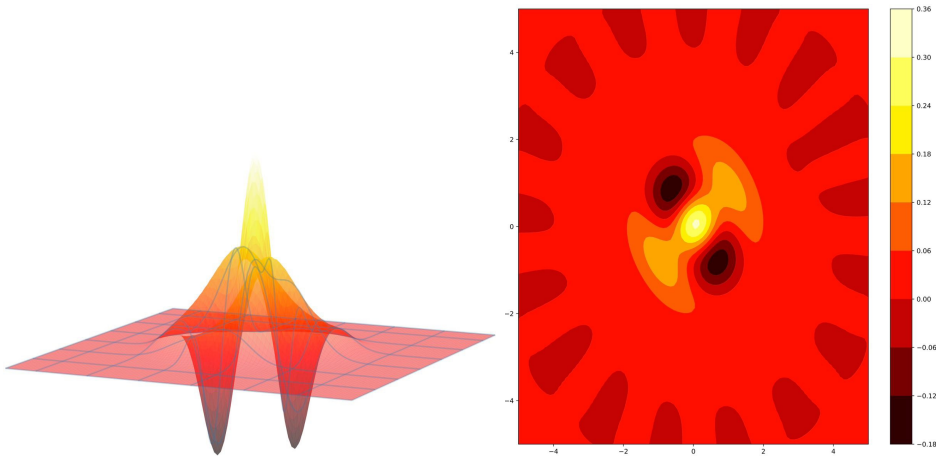

Fig. 3.2 Even Schrodinger cat states in idea conditions[11],[1].

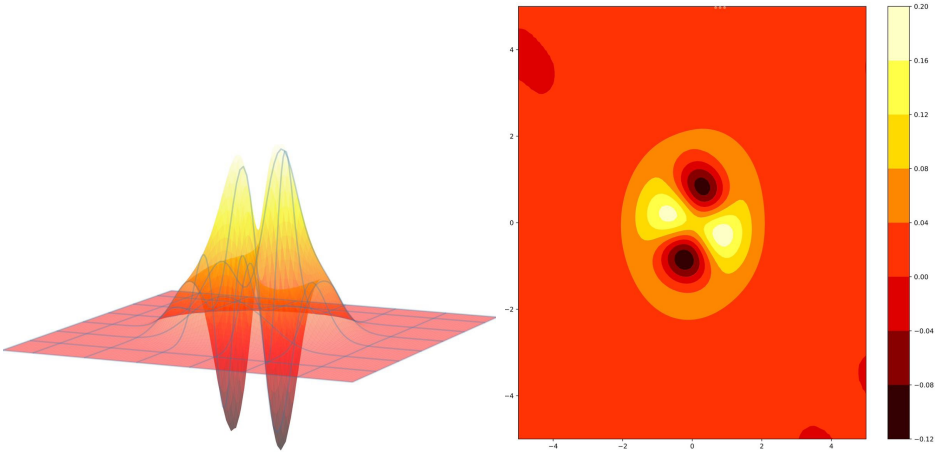

Fig. 3.3 Odd Schrodinger cat states in ideal condition[11],[1].

we introduced dissipation into the system, we observed a notable decrease in fidelity for both even and odd cat states. Specifically, the fidelity for even cat states decreased to 0.65, and for odd cat states, it fell to 0.55.

It is important to note that different types of dissipation can have varying impacts on the fidelity of state preparation. For instance, the decay of the cavity mode can lead to mixing the cat state with other cavity states, whereas spontaneous emission can cause the cat state to collapse rapidly. Therefore, careful consideration of the effects of dissipation is essential in designing an atom-cavity system for preparing cat states.

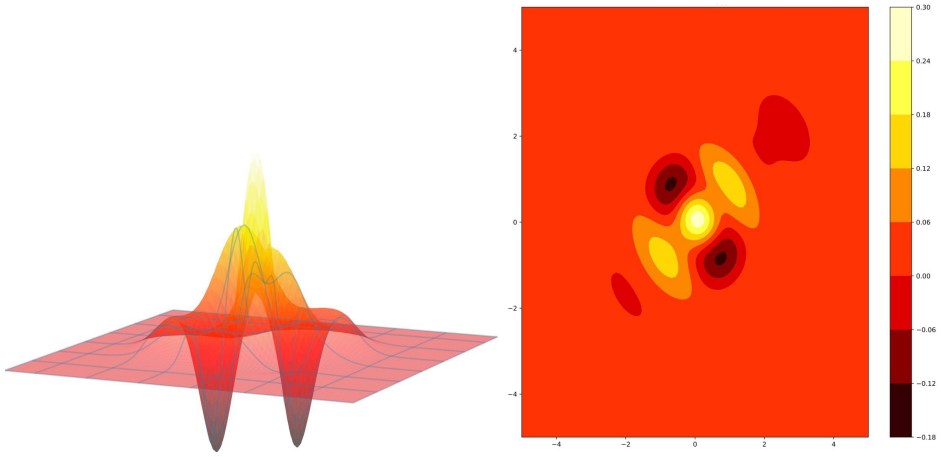

Fig. 3.4 even Schrodinger cat states with decay and cavity losses[11],[1].

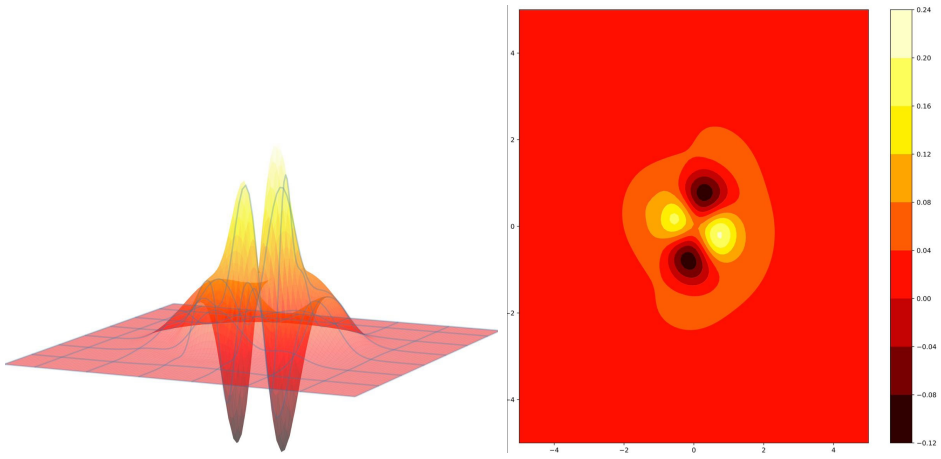

Fig. 3.5 odd Schrodinger cat states with decay and cavity losses[11],[1].

Chapter 4

Conclusion

In this study, we have investigated three different protocols for preparing photonic Schrodinger cat states. We aimed to explore the feasibility of preparing these states in solid-state quantum dot-cavity (QDC) and atom-cavity systems, which have potential applications in quantum information processing and quantum communication.

The first two protocols we investigated were the Deterministic Dot-Driven (DOD) and the Cavity driven (CAD) protocols for generating Schrodinger cat states in the QDC system. We found that both protocols rely heavily on the precise timing and mutual phases of external laser pulses to control the quantum dot and prepare the Schrodinger cat state. However, we also discovered that radiative decay and cavity losses could harm all preparation schemes. In particular, the environmental coupling to longitudinal acoustic phonons significantly impacts the Schrodinger cat state preparation in QDCs. Therefore, theoretical guidance on the feasibility of preparing cat states is essential.

We determined that the DOD protocol was inadequate for generating Schrödinger cats in realistic QDCs due to the negative impact of the Cavity and radiative losses and environmental coupling with longitudinal acoustic phonons. The resulting state is an incoherent mixture of the two macroscopically distinct forms with no non-classicality. Achieving Schrödinger-cat preparation with this protocol in QDCs would require a similar

improvement in the quality factor. On the other hand, the CAD protocol was more effective in preparing Schrödinger cats in QDCs by utilizing the internal dynamics of the Jaynes-Cummings model. In the ideal scenario, this protocol is most successful with high-pulse areas, but losses also increase in such cases, rendering preparation impossible. Although the phonon effects are less severe than in the DOD protocol, the coherences and non-classicality of the Schrödinger cats remain even under the influence of both losses and phonons.

The third protocol we investigated was generating Schrodinger cat states in an atom-cavity system via deterministic entanglement. We found that it is possible to prepare more advanced Schrodinger cat states with this protocol using Ramsey field pulses, which are used to achieve superposition in the atom state and overall superposition in the coherent states. We were able to create even Schrodinger cat states and odd Schrodinger cat states, which are more complicated and advanced Schrodinger cat states. In this protocol, the precise timing of the pulse and their mutual phase are paramount. However, like the QDC protocols, the losses are caused by destroying the cat state.

Our findings demonstrate that Schrödinger cats in QDCs can be prepared with an easy-to-use protocol under realistic conditions. However, a boost of the cavity quality factor would improve the characteristics of the prepared cat state in all protocols. In the atom-cavity system, we prepared more advanced Schrodinger cat states with the help of Ramsey pulses, but losses also played a significant role in this protocol. By investigating these protocols, we have provided a more detailed understanding of the preparation of Schrodinger cat states in both QDCs and atom-cavity systems.

Chapter 5

Appendix

5.1 Environmental coupling Hamiltonian

In real-world scenarios, Quantum Dot Cavities (QDCs) are subject to lose effects, primarily due to the radiative decay of Quantum Dots and the limited quality factor of the cavity. Additionally, Quantum Dots are influenced by longitudinal acoustic phonons, which are recognized as a significant source of decoherence, even at cryogenic temperatures such as T=4K. This presents a fundamental difference between semiconductor-based systems and atomic-based systems. The Hamiltonian that accounts for the coupling of longitudinal acoustic phonons with a Quantum Dot is expressed as follows.

$$\hat{H}_{ph} = \Sigma_k \hbar\omega b_k^\dagger b_k^\dagger + \Sigma_k(\Gamma_k b_k^\dagger + \Gamma_k^\dagger b_k)|E\rangle\langle E|) \tag{5.1}$$

And 2^{nd} part of above Hamiltonian

$$\hat{H}_{d.phase} = \Sigma_k(\Gamma_k b_k^\dagger + \Gamma_k^\dagger b_k)|E\rangle\langle E| \tag{5.2}$$

A Hamiltonian consisting of a pure dephasing term is considered, wherein $b^\dagger k$ and bk are the (bulk) phonon operators with vector k and energy $\hbar\omega_k$, and ω_k is the frequency of the bath oscillators [7]. The Γ_k parameterizes the deformation potential-type coupling to the

electronic state. This dephasing Hamiltonian encompasses the phonon sideband in the QD-emission spectrum, damping of Rabi oscillations, and the recombination of their frequencies. A complete Hamiltonian for a practical scenario can be obtained by summing all the terms.

$$\hat{H}_{full} = \hat{H} + \hat{H}_{ph} \tag{5.3}$$

By defining γ as the radiative recombination rate of the exciton and κ as the cavity loss rate, the Markovian Lindblad-type operator can be employed to describe the system's behavior.

$$\Xi_{G,\zeta^\bullet} = \zeta(G^\bullet G^\dagger - \frac{1}{2}\{\bullet, G^\dagger G\}) \tag{5.4}$$

Assuming G is the system operator, ζ is linked to the loss process's decay rate associated with the system, and $\cdot,\cdot$ represents the anticommutator, and the system's dynamics can be expressed using the Liouville-von Neumann equation

$$\frac{\delta}{\delta t}\rho = -\frac{\iota}{\hbar}[\hat{H}_{full}, \rho] + \zeta_{\hat{a},\kappa}\rho + \zeta_{\sigma_X,\gamma}\rho, \tag{5.5}$$

Where ,$[\cdot,\cdot]$ is commutator.

5.2 Parameters

Fig. 5.1 Relevant system parameters[3]

QD-cavity coupling (meV)	$\hbar g$	0.1
Cavity loss rate (ps^{-1})	κ	0.0085
QD radiative decay rate (ps^{-1})	γ	0.001

To perform numerical computations, GaAs/In(Ga)As quantum dots are utilized, with the cavity's quality factor being approximately $Q \approx 268000$ at a mode frequency of $\hbar\omega_c = 1.5$eV. The entire system is assumed to be in thermal equilibrium with a temperature of 4 Kelvin, and additional pertinent parameters are listed in figure(5.1)[3].

References

[1] Ari, N., and Ustazhanov, M. Matplotlib in python. In *2014 11th International Conference on Electronics, Computer and Computation (ICECCO)* (2014), IEEE, pp. 1–6.

[2] Cirac, J., Parkins, A., Blatt, R., and Zoller, P. Nonclassical states of motion in ion traps. In *Advances in Atomic, Molecular, and Optical Physics*, vol. 37. Elsevier, 1996, pp. 237–296.

[3] Cosacchi, M., Seidelmann, T., Wiercinski, J., Cygorek, M., Vagov, A., Reiter, D., and Axt, V. M. Schrödinger cat states in quantum-dot-cavity systems. *Physical Review Research 3*, 2 (2021), 023088.

[4] Duan, L.-M., Lukin, M. D., Cirac, J. I., and Zoller, P. Long-distance quantum communication with atomic ensembles and linear optics. *Nature 414*, 6862 (2001), 413–418.

[5] Gea-Banacloche, J. Collapse and revival of the state vector in the jaynes-cummings model: An example of state preparation by a quantum apparatus. *Physical review letters 65*, 27 (1990), 3385.

[6] Gerry, C., and Knight, P. Quantum superpositions and schrödinger cat states in quantum optics. *American Journal of Physics 65*, 10 (1997), 964–974.

[7] Gerry, C., Knight, P., and Knight, P. L. *Introductory quantum optics*. Cambridge university press, 2005.

[8] Gisin, N., Ribordy, G., Tittel, W., and Zbinden, H. Quantum cryptography. *Reviews of modern physics 74*, 1 (2002), 145.

[9] Hacker, B., Welte, S., Daiss, S., Shaukat, A., Ritter, S., Li, L., and Rempe, G. Deterministic creation of entangled atom–light schrödinger-cat states. *Nature Photonics 13*, 2 (2019), 110–115.

[10] Jacak, L., Hawrylak, P., and Wojs, A. *Quantum dots*. Springer Science & Business Media, 2013.

[11] Johansson, J. R., Nation, P. D., and Nori, F. Qutip: An open-source python framework for the dynamics of open quantum systems. *Computer Physics Communications 183*, 8 (2012), 1760–1772.

[12] Joo, J., Munro, W. J., and Spiller, T. P. Quantum metrology with entangled coherent states. *Physical review letters 107*, 8 (2011), 083601.

[13] Jozsa, R. Fidelity for mixed quantum states. *Journal of modern optics 41*, 12 (1994), 2315–2323.

[14] Law, C. K., and Eberly, J. H. Arbitrary control of a quantum electromagnetic field. *Physical review letters 76*, 7 (1996), 1055.

[15] Ralph, T. C., Gilchrist, A., Milburn, G. J., Munro, W. J., and Glancy, S. Quantum computation with optical coherent states. *Physical Review A 68*, 4 (2003), 042319.

[16] Schrödinger, E. Die gegenwärtige situation in der quantenmechanik. *Naturwissenschaften 23*, 50 (1935), 844–849.

[17] Scully, M. O., and Zubairy, M. S. Quantum optics, 1999.

[18] Shore, B. W., and Knight, P. L. The jaynes-cummings model. *Journal of Modern Optics 40*, 7 (1993), 1195–1238.

[19] Thomas-Peter, N., Smith, B. J., Datta, A., Zhang, L., Dorner, U., and Walmsley, I. A. Real-world quantum sensors: evaluating resources for precision measurement. *Physical review letters 107*, 11 (2011), 113603.

[20] van Enk, S. J., and Hirota, O. Entangled coherent states: Teleportation and decoherence. *Physical Review A 64*, 2 (2001), 022313.